https://doi.org/10.5194/amt-2023-245
Preprint. Discussion started: 6 December 2023

Atmospheric Measurement Techniques Discussions

Field comparison of dual- and single-spot aethalometers: Equivalent black carbon, light absorption, Ångström exponent and secondary brown carbon estimations

Liangbin Wu[1,2,3], Cheng Wu[1,2,3*], Tao Deng[4], Dui Wu[1,2,3], Mei Li[1,2,3], Yong Jie Li[5], Zhen Zhou[1,2,3]

[1]Institute of Mass Spectrometry and Atmospheric Environment, Guangdong Provincial Engineering Research Center for online source apportionment system of air pollution, Jinan University, Guangzhou 510632, China

[2]Guangdong-Hongkong-Macau Joint Laboratory of Collaborative Innovation for Environmental Quality, Guangzhou 510632, China

[3]Guangdong MS Institute of Scientific Instrument Innovation, Guangzhou 510530, China

[4]Institute of Tropical and Marine Meteorology, CMA, Guangzhou 510080, China

[5]Department of Civil and Environmental Engineering, Centre for Regional Oceans, and Department of Ocean Science and Technology, Faculty of Science and Technology, University of Macau, Taipa, Macau, China

Correspondence to: Cheng WU (wucheng.vip@foxmail.com)

Abstract. Aethalometer is a widely used instrument for black carbon (BC) mass concentration and light absorption coefficient (b_{abs}) measurements around the world. However, field intercomparison of the two popular models, dual-spot (AE33) and single-spot (AE31) aethalometers, remain limited; in addition, the difference in secondary brown carbon (BrC_{sec}) light absorption estimation between the two models is largely unknown. We performed full-year collocated AE33 and AE31 measurements in a megacity in southern China – Guangzhou. The b_{abs} values agree well between the two aethalometers ($R^2 > 0.95$), with AE33/AE31 slopes ranging from 0.87 to 1.04 for 7 wavelengths. AE33 consistently exhibits lower limits of detection (LOD) than AE31 for time resolutions of 2 to 60 min. The AE33/AE31 slope for equivalent BC (eBC) was 1.2, implying the need for site-specific post-correction. The Ångström exponent (AAE) obtained from different approaches agrees not very well between the two models, with the biggest discrepancy found in $AAE_{880/950}$. The estimated BrC_{sec} light absorption at 370 nm (b_{abs370_BrCsec}) was calculated using the minimum *R* squared method (MRS) for both Aethalometers. The b_{abs370_BrCsec} comparison yields a slope of 0.78 and an R^2 of 0.72 between the two models, implying a non-negligible inter-instrument difference. This study highlights the high consistency in b_{abs} but less so in AAE between AE31 and AE33, and reveals site-specific correction for eBC estimation and non-negligible difference in BrC_{sec} estimation. The results are valuable for data continuity in long-term aethalometer measurements

https://doi.org/10.5194/amt-2023-245
Preprint. Discussion started: 6 December 2023

Atmospheric Measurement Techniques Discussions

when transiting from the older (AE31) to the newer (AE33) model, as anticipated in permanent global-climate and air-quality stations.

Keywords:

Black carbon, aethalometer, light absorption coefficient, correction algorithm, secondary brown carbon light absorption

1. Introduction

Black carbon (BC) and organic carbon (OC) are important carbonaceous aerosol components in the atmosphere, and they play an important role in both global climate and air quality (Bond and Bergstrom, 2006; Li et al., 2021). BC is an important short-lived climate forcer owing to its strong absorption of solar radiation over a wide wavelength range (Bond et al., 2013). A specific group of OC exhibits strong light absorption in the ultraviolet band and the light absorption decreases with increasing wavelength (Jacobson, 1999), which is later termed as brown carbon (BrC) due to its brown color appearance (Andreae and Gelencser, 2006). Previous studies have shown that BrC accounts for about 20% of the total carbonaceous aerosol light absorption (Feng et al., 2013; Wang et al., 2014; Jo et al., 2016). Light absorption is an important characteristic of BrC, but the current knowledge of BrC is still limited due to the complexity of its chemical composition (Huang et al., 2018). Unlike BC which was solely emitted from primary sources, BrC can be formed secondarily in the atmosphere (Moise et al., 2015; Laskin et al., 2015). Secondary BrC (BrC_{sec}) can be formed via various pathways, e.g., nitration of aromatic compounds (NACs) (Lin et al., 2017), aqueous reactions (Lian et al., 2021; Tang et al., 2016), droplet evaporation (Lee et al., 2013), iron-catalyzed reactions (Al-Abadleh, 2021), etc. During the atmospheric aging process, the light absorption of BrC can be either enhanced or reduced (Li et al., 2023), depending on whether the chromophores are destroyed (e.g., fragmentation) or re-built (e.g., dimerization) (Jiang et al., 2022).

Filter-based technique (Rosen et al., 1980) has been widely used for aerosol light absorption measurement since its introduction in the early 1980s, due to its low operational cost and ease of maintenance (Moosmüller et al., 2009). The aethalometer (Hansen et al., 1984) is the most commonly used instrument for aerosol light absorption measurement (Lack et al., 2014). Measurement artifacts using the filter-based approach due to the loading effect and multi-scattering effect, however, can bias the results of the aethalometer (Coen et al., 2010). To tackle these issues, various correction algorithms

https://doi.org/10.5194/amt-2023-245
Preprint. Discussion started: 6 December 2023

Atmospheric Measurement Techniques Discussions

have been introduced (Weingartner et al., 2003; Arnott et al., 2005; Schmid et al., 2006; Virkkula et al., 2007; Li et al., 2020; Zhang et al., 2021b). It is widely recognized that careful post-correction is essential for the accurate light absorption determination by the aethalometer. Intercomparisons between the aethalometer and the reference method (e.g., photoacoustic spectroscopy, PAS) have shown that a collocated study is needed to determine the site-specific multi-scattering correction factor (C_{ref}) (Arnott et al., 2005; Kim et al., 2018; Zhao et al., 2020). AE31 and AE33 (Aerosol Magee Scientific, CA, USA) are the two most widely used aethalometers nowadays. Both instruments can provide filter-based measurements at 7 wavelengths, but AE33 has the embedded dual-spot technique to perform real-time loading effect correction (Drinovec et al., 2015), while AE31 requires manual post-correction by the user. The intercomparison of these two models has been investigated (Titos et al., 2015; Rajesh and Ramachandran, 2018; Ferrero et al., 2021). These studies mainly focus on the eBC comparison, while b_{abs} comparison was rarely reported (Asmi et al., 2021). In addition, two questions remain unanswered. 1) How does the AE33/AE31 comparison slope vary throughout a long-term measurement period, e.g., a year? Existing AE33/AE31 intercomparisons only cover a few months (Table 1), leaving the seasonality of the intercomparison not well characterized. 2) The inter-instrument bias of BrC_{sec} light absorption (b_{abs_BrCsec}) between AE31 and AE33 has not been investigated. A newly established minimum R squared (MRS) method for b_{abs_BrCsec} determination using aethalometer data (Wang et al., 2019a) has gained popularity in recent aethalometer studies (Zhu et al., 2021a; Guo et al., 2022; Ivančič et al., 2022; Lei et al., 2023). However, the difference in b_{abs_BrCsec} determination between AE31 and AE33 remains unknown.

This study aims to fill the aforementioned knowledge gaps. Colocated intercomparison of the AE31 and AE33 was conducted at an urban site in a megacity in southern China (Guangzhou, the capital of the Guangdong province) for one full year. Several metrics were characterized and compared between AE31 and AE33, including limits of detection (LOD), light absorption coefficient, equivalent BC (eBC) mass concentration and absorption Ångström exponent (AAE). The difference in b_{abs_BrCsec} between AE31 and AE33 was also evaluated using the MRS method. The impacts of the data correction schemes, seasonality, and temporal resolution was were investigated.

2. Methods

2.1 Observation site and measurement period

https://doi.org/10.5194/amt-2023-245
Preprint. Discussion started: 6 December 2023

Atmospheric Measurement Techniques Discussions

The measurements of sampling were performed in the Jinan University atmospheric supersite (JNU, 23.13° N, 113.35° E; 40 m above sea level), which lies in the central business district of Guangzhou. The measurement site is on top of the library building and surrounded by the teaching building and residential areas (Liang et al., 2021). The campus is surrounded by three busiest roads in the city, and traffic emissions are a major source of local air pollutants. Guangzhou is situated in the south of China and is the geographical and business center of the Guangdong province as well. Therefore, the JNU site can represent a typical urban environment in the Pearl River Delta (PRD) region. The measurement period of colocated intercomparison covers one year, from April 2021 to March 2022.

2.2 Instruments and data correction

Two aethalometers were compared in this study, a single spot Aethalometer (AE31, Magee Scientific, CA, USA), and a dual-spot aethalometer (AE33, Magee Scientific, CA, USA). The single-spot AE31 was operated at a flow rate of 2.4 $L \cdot min^{-1}$ using the quartz fiber filter tape (Pallflex, type Q250F). The dual-spot AE33 measurement was conducted at a flow rate of 3 $L \cdot min^{-1}$ using filter tape 8060. The data acquisition time base was 5 min and 1 min, for AE31 and AE33, respectively. Both AE31 and AE33 were connected to one $PM_{2.5}$ inlet. An inline Nafion dryer (MD-700, Perma Pure, NJ, USA) was used to minimize the impact of relative humidity. Both AE31 and AE33 were set to advance the filter tape to a new spot when the light attenuation (ATN) at 370 nm reached 100.

2.2.1 Single-spot aethalometer - AE31

The AE31 measures light attenuation (ATN) at seven wavelengths (370, 470, 520, 590, 660, 880, and 950 nm) through a particle-laden filter. ATN can be calculated by the Beer-Lambert law:

$$ATN = -100 \cdot \ln(I/I_0) \quad (1)$$

where I and I_0 are the intensities of light transmitted through the particle-laden filter and particle-free filter, respectively. The aerosol sample is continuously deposited on the filter, leading to the increase of ATN over time. The light attenuation coefficient (b_{ATN}) for particles collected on the filter tape is defined as follows:

$$b_{ATN} = \frac{A}{F} \cdot \frac{\Delta ATN}{\Delta t} \quad (2)$$

where A is the sample spot aera, F is the aerosol flow rate and the ΔATN is the change of ATN over a time period Δt. It is worth noting that the b_{ATN} differs from the aerosol light absorption coefficient (b_{abs})

https://doi.org/10.5194/amt-2023-245
Preprint. Discussion started: 6 December 2023

Atmospheric Measurement Techniques Discussions

because it is determined by the ATN through the particle-laden filter, and the discrepancy can be reconciled by different algorithms (Coen et al., 2010). Then eBC_{raw} can be calculated from:

$$eBC_{raw} = \frac{b_{ATN}}{\sigma_{ATN}} \quad (3)$$

Here σ_{ATN} is the conversion factor between b_{ATN} and eBC, and the values of σ_{ATN} at 7 wavelengths recommended by the manufacturer can be found in Table S1.

In this study, two data correction algorithms were applied and compared, including Weingartner (Weingartner et al., 2003) and Virkkula (Virkkula et al., 2007). Both Weingartner and Virkkula corrections were implemented for AE31 data using an Igor Pro based toolkit (Aethalometer Data Processor) (Wu et al., 2018).

The Weingartner scheme is defined as follows:

$$eBC_{corrected} = \frac{eBC_{raw}}{R(ATN)} \quad (4)$$

$$R(ATN) = \left(\frac{1}{f} - 1\right) \cdot \frac{ln(ATN) - ln(10)}{ln(50) - ln(10)} + 1 \quad (5)$$

$eBC_{corrected}$ is mass concentration after loading correction. *R(ATN)* is the correction fucntion for the loading effect and *f* is the empirical filter loading effect compensation parameter.

The Virkkula correction can be calculated as follows:

$$eBC_{corrected} = (1 + k \cdot ATN) \cdot eBC_{raw} \quad (6)$$

where k_i is the loading effect compensation parameter for the i^{th} sampling spot that can be calculated from the following equation:

$$k_i = \frac{eBC_{raw}(t_{i+1,\text{first}}) - eBC_{raw}(t_{i,\text{last}})}{ATN(t_{i,\text{last}}) \cdot eBC_{raw}(t_{i,\text{last}}) - ATN(t_{i+1,\text{first}}) \cdot eBC_{raw}(t_{i+1,\text{first}})} \quad (7)$$

where eBC_{raw} is the raw BC concentration before correction, ATN is light attenuation, $t_{i,\text{last}}$ refers to the last measurement data for filter spot i, and $t_{i+1,\text{first}}$ refers to the first measurement data for the next filter spot. An example of AE31 data before and after correction is shown in Figure S1. It is very clear that data discontiuety during filter advance was effectively minimized by both algorithms.

Once $eBC_{corrected}$ was obtained either by Weingartner or Virkkula algorithm, the corresponding light absorption coefficient (b_{abs}) can be back-calculated from

$$b_{abs}\ (AE31) = \frac{eBC_{corrected} \cdot \sigma_{ATN}}{C_{ref}} \quad (8)$$

https://doi.org/10.5194/amt-2023-245
Preprint. Discussion started: 6 December 2023

Atmospheric Measurement Techniques Discussions

where b_{abs} is the aerosol light absorption coefficient in the air, C_{ref} is the multiple scattering parameter, whose value depends on the filter material and mixing state of the particles (coating thickness). For example, C_{ref} = 3.6 ± 0.6 was observed in the organic coating experiment using a quartz filter (Weingartner et al., 2003). In this study, C_{ref} = 3.48 was adopted for AE31 according to a previous intercomparison study between aethalometer and PAS in Guangzhou (Wu et al., 2013). This value is similar to those recommended by the guidelines from the Global Atmosphere Watch Programme (C_{ref} = 3.5) (WMO/GAW, 2016).

2.2.2 Dual-spot aethalometer – AE33

AE33 collects particles on two spots with different flow rates, leading to a different ATN increase over time (Drinovec et al., 2015), thus the b_{ATN} of the two spots can be calculated from:

$$b_{ATN1} = \frac{A}{F1} \cdot \frac{\Delta ATN1}{\Delta t} \quad (9)$$

$$b_{ATN2} = \frac{A}{F2} \cdot \frac{\Delta ATN2}{\Delta t} \quad (10)$$

where A is the sample spot aera, and F_1 and F_2 are the flow rates at the two sampling spots, with a ratio of 2:1. $\Delta ATN1$ and $\Delta ATN1$ are the changes of ATN over a time period Δt at the two spots. The raw BC concentration can be calculated from:

$$eBC1_{raw} = \frac{b_{ATN1}}{C_{AE33} \cdot \sigma_{air}} \quad (11)$$

$$eBC2_{raw} = \frac{b_{ATN2}}{C_{AE33} \cdot \sigma_{air}} \quad (12)$$

C_{AE33} is the multiple scattering parameter provided by the manufacturer, which strongly depends on the material of the filter tape. For example, C_{AE33}=1.57 was used for tape model 8020 and 8050, while C_{AE33}=1.39 should be applied for tape 8060 (Magee-Scientific, 2017), which is the case of the current study. Here σ_{air} is the conversion factor between b_{ATN} and eBC, and the values of σ_{air} of AE33 at 7 wavelengths recommended by the manufacturer can be found in Table S1.

With known ATN and raw eBC concentrations of the two spots, the corrected eBC can be calculated from the dual-spot equations (Drinovec et al., 2015):

$$eBC1_{raw} = eBC_{corrected} \cdot (1 - k \cdot ATN1) \quad (13)$$

$$eBC2_{raw} = eBC_{corrected} \cdot (1 - k \cdot ATN2) \quad (14)$$

Here k is the loading effect compensation parameter. It should be noted that k in Virkkula correction of

https://doi.org/10.5194/amt-2023-245
Preprint. Discussion started: 6 December 2023

Atmospheric Measurement Techniques Discussions

AE31 data is a constant for all data points within each tape advance cycle, while k in the dual-spot correction of the AE33 data is a variable that can be calculated for every data point. By solving the two equations, both k and $eBC_{corrected}$ can be determined. An example of AE33 data before and after correction is shown in Figure S1. It is very clear that data discontinuity during filter advance was successfully minimized by the dual-spot algorithms.

Once $eBC_{corrected}$ is determined, b_{abs} can be back calculated from:

$$b_{abs}\ (AE33) = \frac{eBC_{corrected} \cdot \sigma_{air}}{C'} \quad (15)$$

Here σ_{air} is the conversion factor between b_{ATN} and eBC, the values of σ_{air} of AE33 at 7 wavelengths recommended by the manufacturer can be found in Table S1. As suggested by a previous study in Guangzhou, the C_{AE33} recommended by the manufacturer is not sufficient to achieve a 1:1 slope with the reference instrument, thus a second correction factor C'=2.1 was introduced (Qin et al., 2018). A study in central Oregon of USA also found that C_{AE33}=1.57 by default is too low and C_{ref} =4.35 was recomended (Laing et al., 2020). Therefore, a final correction factor of $C_{ref} = C_{AE33} \cdot C'$=2.919 (filter tape 8060) is used for AE33 in this study. This value is very close to the value (C_{ref} = 2.9 ± 0.4, filter tape 8060) found in eastern China (Zhao et al., 2020) (Table S2), but slightly higher than those used by European ACTRIS measurement network (C_{ref} = 2.45, filter tape 8060) (Savadkoohi et al., 2023)

2.2.3 Absorption Ångström exponent

Absorption Ångström exponent (AAE) is a useful parameter that characterize the wavelength dependence of particle absorption. AAE can be calculated from two approaches and previous studies have shown that the two approaches can lead to different results (Lack and Cappa, 2010; Helin et al., 2021). The first approach involves calculations using two wavelengths:

$$AAE_{\lambda 1/\_\lambda 2} = -\frac{\ln(b_{abs\_\lambda 1}) - \ln(b_{abs\_\lambda 2})}{\ln(\lambda_1) - \ln(\lambda_2)} \quad (16)$$

where $AAE_{\lambda 1/\_\lambda 2}$ is the absorption Ångström exponent, and $b_{abs\_\lambda 1}$ and $b_{abs\_\lambda 2}$ are the light absorption coefficients at wavelength λ_1 and wavelength λ_2, respectively.

The second approach utilizes all available wavelengths in a specific range by power-law curve fitting. Detailed calculation examples are given in Text S1 in the SI. To distinguish the AAE values calculated from these two approaches, different notations were used. For example, $AAE_{370/950}$ refers to the AAE calculated by Approach 1, while $AAE_{370\text{-}950}$ represents the AAE determined by Approach 2 using all wavelengths data between 370 and 950 nm (seven wavelengths for both AE31 and AE33). This

https://doi.org/10.5194/amt-2023-245
Preprint. Discussion started: 6 December 2023

Atmospheric Measurement Techniques Discussions

notation emphasizes that "/" represents the separator of the two wavelengths in Approach 1 and "-" denotes the range of wavelength in Approach 2.

2.2.4 Light absorption of secondary brown carbon

The secondary brown carbon light absorption at 370 nm (b_{abs370_BrCsec}) was calculated using the minimum *R* squared (MRS) method (Wu and Yu, 2016; Wang et al., 2019a). First, the b_{abs} can be divided into two parts: secondary brown carbon light absorption ($b_{abs\_\lambda\_BrCsec}$) and non-secondary brown carbon light absorption ($b_{abs\_\lambda\_other}$) at wavelength λ:

$$b_{abs\_\lambda} = b_{abs\_\lambda\_BrCsec} + b_{abs\_\lambda\_other} \quad (17)$$

where b_{abs_λ} is the total light absorption at wavelength λ from direct measurements. It is generally believed that the light absorption of BrC is negligible at the wavelength of 880 nm, and the BrC_{sec} is generated during the secondary aging process. Therefore it is assumed that the BrC_{sec} is not correlated with BC. Based on this assumption, the light absorption at 880 nm can be used as a tracer to characterize the $b_{abs\_\lambda\_other}$ at shorter wavelengths (e.g., 370 to 660 nm) :

$$b_{abs\_\lambda\_other} = \left(\frac{b_{abs\_\lambda}}{b_{abs\_880}}\right)_{pri} \times b_{abs\_880} \quad (18)$$

where b_{abs_880} is the light absorption coefficient at 880 nm. The key parameter here is the primary ratio $(b_{abs\_\lambda}/b_{abs\_880})_{pri}$, which can be calculated using the Igor-based MRS toolkit (Wu and Yu, 2016). As a result, the $b_{abs\_\lambda\_BrCsec}$ can be determined as follows:

$$b_{abs\_\lambda\_BrCsec} = b_{abs\_\lambda} - \left(\frac{b_{abs\_\lambda}}{b_{abs\_880}}\right)_{pri} \times b_{abs\_880} \quad (19)$$

2.2.5 Error-in-variables linear regression

Conventional ordinary least squares (OLS) assume that independent variables (X) are error-free. However, for inter-instrument comparison studies, X and Y (from two instruments) usually have comparable degrees of uncertainty. In this case, linear regression by OLS should be avoided as biased slope and intercept will be resulted. To account for uncertainties in both X and Y, an error-in-variables linear regression technique, weighted orthogonal distance regression (WODR), was applied in this study, implemented by the Igor-based toolkit Scatter Plot (Wu and Yu, 2018).

3. Results and discussions

3.1 eBC concentration comparison

https://doi.org/10.5194/amt-2023-245
Preprint. Discussion started: 6 December 2023

Atmospheric Measurement Techniques Discussions

The limits of detection (LOD) of eBC of the AE31 and AE33 aethalometers were derived from three times the standard deviation of the blank measurements. The blanks were obtained by placing a HEPA filter upstream of the two aethalometers. During the experiment, the time bases of both instruments were set to their highest time resolution (1 s for AE33 and 2 min for AE31) with a sampling flow rate of 5L·min^{-1}. In total, 96-h blank data was obtained for both aethalometers.

To investigate the LOD of eBC at different time resolutions, data averaging was performed at various time bases as summarized in Table 2. It is clear that the LOD decreases with increased data averaging interval. For example, 370 nm eBC LOD of AE33 was 553.67 ng m^{-3} at 1 s and can be reduced to 82.17 ng m^{-3} if the time base was changed to 1 min. For the same time base, eBC LOD increases with longer wavelengths. As the newer model, AE33 exhibits a lower eBC LOD at all wavelengths. For example, 370 nm eBC LOD were 75.42 and 197.01 ng m^{-3} at 2 min for AE33 and AE31, respectively (Figure 1). The AE33/AE31 LOD difference becomes smaller for longer time intervals. For example, the 370 nm LOD at 60 min were 14.25 and 20.82 ng m^{-3}, for AE33 and AE31, respectively (Figure S2a). In addition, the LOD difference between 370 nm and 950 nm of AE33 (e.g., 75.42 vs. 99.72 ng m^{-3} @ 2 min) was much smaller than that of AE31 (e.g., 197.01 vs 789.99 ng m^{-3}@ 2 min) as shown in Table 2. In other words, the AE33 LOD improvement was more pronounced at longer wavelengths (e.g. 96.57 vs. 730.68 ng m^{-3} @ 880 nm, 2 min, for AE33 and AE31, respectively) as shown in Table 1 and Figure 1f. In summary, the LOD performance was significantly improved on AE33, especially for the infrared (IR) channels (880 and 950 nm), which were commonly used for reporting eBC concentrations.

Among the 7 wavelengths, 880 nm is recognized as the standard wavelength for reporting eBC concentration, since interference of BrC and dust on BC determination can be minimized in the IR range. We therefore discuss the eBC comparison at 880 nm in this section. To maintain consistent long-term eBC measurement results, the older model (AE31) was selected as the reference instrument. For this reason, AE31 data was set as the X variable and the AE33 data was set as the Y variable in the linear regression (Figure 2). To investigate the effect of data correction schemes, AE31 results from both Virkkula and Weingartner corrections were included in the comparison. As shown in Figure 2, hourly eBC from the two aethamometers agree very well, with high R^2 values (0.96~0.97) and a slope of 1.2 (Figures 2a&b). The 5 min data yield similar results, with a slope of 1.18 and R^2 of 0.91 (Figure 2d&e). The annual average eBC by AE31 for 1 hr and 5 min data were 1.95±1.12 and 1.96±1.18 μg m^{-3},

https://doi.org/10.5194/amt-2023-245
Preprint. Discussion started: 6 December 2023

Atmospheric Measurement Techniques Discussions

respectively. The annual average eBC by AE33 for 1 hr and 5 min data were identical (2.35 μg m^{-3}). These results imply that the inter-instrument slope and annual mean of eBC are not sensitive to the time resolution of the data. The inter-instrument eBC slope obtained in this study is higher than those found in previous studies, as summarized in Table 1. A slope of 1.11 was observed in a 2-month study at an urban site in Spain. Similar results were reported elsewhere, e.g., slope=1.02 from a 6-month study in urban India (Rajesh and Ramachandran, 2018) and slope=1.05 from a 1-month study in urban Italy (Ferrero et al., 2021). The ~20% bias in the slope found in this study suggests that the AE33/AE31 slope could be site dependent. As a result, post-adjustment is needed to obtain consistent results from the two aethalometers.

To maintain the consistency of the historical data of AE31, the eBC mass concentration of AE33 aethalometer was further adjusted by a second correction factor (C_{eBC}, 1.20 and 1.18 for 1 hr and 5 min data, respectively), which is the slope obtained in Figure 2:

$$eBC_{2nd\_cor} = \frac{eBC}{C_{eBC}} \quad (20)$$

After the eBC correction, the annual averages of the two instruments were also in good agreement as shown in Figure 3. The annual mean eBC obtained from 1 hr AE33 data were 2.35±1.37 and 1.96±1.14 μg m^{-3}, respectively, before and after eBC correction (Table S3). The latter value agrees well with the AE31 annual average (1.95±1.12 μg m^{-3}, Table S3). In summary, fine-tuning of the AE33 data by applying a site-specific inter-instrument correction factor (C_{eBC}) is needed to maintain the consistency of the historical data from AE31.

3.2 Intercomparison of light absorption coefficient

Light absorption coefficient by the two aethalometers was compared, including AE31 data corrected by Virkkula (AE31_V_b_{abs}) and Weingartner (AE31_W_b_{abs}) algorithms and AE33 results (AE33_b_{abs}). The differences in b_{abs} annual mean between AE33 and AE31 is small across 7 wavelengths (Table S4). The year-long hourly b_{abs} of the two aethalometers agree well, as evidenced by the high R^2 (0.95~1) and close-to-unity slope (0.87~1.04) as shown in Figure 4. The slopes for AE33_b_{abs} vs. AE31_V_b_{abs} vary slightly by wavelengths, ranging from 0.87 to 0.97 (Figure 4). The AE33/AE31 agreement on b_{abs660} observed in this study (slope=0.89, Figure 4m) is much better than a previous study (slope=0.47) conducted in the polar region (Asmi et al., 2021), presumably because of the high loadings of light-

https://doi.org/10.5194/amt-2023-245
Preprint. Discussion started: 6 December 2023

Atmospheric Measurement Techniques Discussions

absorbing aerosol particles at this urban site. The comparisons from the AE33_b_{abs} vs. AE31_W_b_{abs} data yield similar results (slope 0.87~1.04), which implies that inter-instrument comparison results between AE33 and AE31 are not sensitive to the data correction schemes used for AE31. The inter-instrument b_{abs} divergence at different wavelengths may be associated with the difference in filter tape material, optical chamber design of aethalometers, as well as the optical properties of aerosols. A study by Yus-Díez et al. (2021) in Spain found that C_{ref} value at IR wavelength was higher than those at UV wavelength when the single scaterring albedo (SSA) was higher than a specific threshold, which was attributed to the presence of dust from the Sahara. But if SSA was lower than a specific threshold, C_{ref} exhibited no dependence on the wavelength. A study in Italy (Bernardoni et al., 2021) found that C_{ref} strongly depended on filter tape material and the wavelength dependence is small. Thus these factors could contribute to the inter-instrument b_{abs} difference at different wavelengths. On-site determination of wavelength-specific C_{ref} is expected to further improve the AE33 vs. AE31 agreement in b_{abs}. However, the wavelengths of existing commercially available multi-wavelength reference instruments (e.g., PAX, PAAS and DPAS) do not fully cover the range of aehtalometers (370–950 nm), which makes such a study very challenging. Nonetheless, the b_{abs} agreement between AE31 and AE33 in this study is good enough despite a single C_{ref} was adopted from previous studies (Table S2).

To investigate the effect of the data correction algorithm on AE31 data, the comparison of AE31_W vs. AE31_V was also conducted as shown in Figure 4. The close-to-unity slopes (0.97~0.99) were observed from 470 to 950 nm, while the slope at 370 nm exhibits a slight bias (0.93). The high R^2 (0.99~1) values found at all seven wavelengths suggest that the results from both algorithms agree very well.

Besides hourly results, b_{abs} intercomparison was also conducted for 5 min data and yields similar slopes (0.85~1.03) as illustrated in Figure S3. The R^2 values (0.89~1) of 5 min data were slightly lower than those of 1 hr data sets as expected, since the increase of data averaging interval can lead to higher inter-instrument R^2 values.

To investigate the monthly variability of AE33 vs. AE31 b_{abs} comparison, linear regression was also performed for individual months as shown in Figure 5. The monthly trend of slope variations between AE33 vs. AE31_V and AE33 vs. AE31_W is identical, which is higher in October and November and lower in July. In addition, no monthly variations were observed for the AE31W vs. AE31_V comparison. These results imply that monthly variations of the AE33 vs. AE31 slopes are not sensitive to the

https://doi.org/10.5194/amt-2023-245
Preprint. Discussion started: 6 December 2023

Atmospheric Measurement Techniques Discussions

correction schemes used for the AE31 data. The monthly trend of slope variations was similar between 5 min and 1 hr data, and the main difference is the increased R^2 values in the 1 hr data (Table S5 and S6). The maximum relative slope deviation of individual months comparing to the annual average was 12.62% and 16.28% for 370 and 880 nm, respectively (Table S7). The results suggest that b_{abs} comparison between AE33 and AE31 exhibits observable monthly variations, but the degree of monthly variations is relatively small.

3.3 Inter-instrument comparison of absorption Ångström exponent

The AAE was widely recognized as a useful indicator for differentiating BC and BrC (Zheng et al., 2021; Wang et al., 2021a), as well as mixing state (Lack and Langridge, 2013). However, inter-instrument comparisons of AAE between different models of aethalometers were rarely reported. In addition, a previous study has shown that using two approaches (Approach 1, using two wavelengths, and Approach 2 power-law fiiting using all wavelengths) for AAE determination may impact the results and even affect the interpretation (Lack and Cappa, 2010). To gain further insights on AAE determination, the AAE values obtained by the two approaches (Approach 1: $AAE_{470/660}$, $AAE_{370/880}$, $AAE_{880/950}$, $AAE_{370/950}$, and Approach 2: $AAE_{370\text{-}950}$) using data from AE31_V, AE31_W and AE33 were compared, as shown in Figure 6 and Table 3.

The inter-instrument R^2 values of AAE were lower than those of b_{abs} and eBC, as shown in Figure 6. In general, the AAE of AE31 data by Virkkula correction correlates better with AE33 data than with Weingartner correction. For example, for $AAE_{370/880}$, the R^2 of AE33 vs. AE31_V (0.56, Figure 6d) was higher than the R^2 of AE33 vs. AE31_W (0.40, Figure 6e). The best inter-instrument AAE agreement was observed in $AAE_{370/880}$, $AAE_{370/950}$ and $AAE_{370\text{-}950}$ for the AE33 vs. AE31_V comparison, with a R^2 of 0.56, 0.52 and 0.63 respectively. The AAE values obtained from 5 min and 1 hr data were almost identical (Figure S4, S5, and Table 3), implying that AAE determination is not sensitive to the time resolution of b_{abs} data.

A previous study by Zhang et al. (2019) suggested that $AAE_{880/950}$ can be used to represent the AAE of BC from fossil-fuel combustion (AAE_{BC}) for the AE33 data. The feasibility of this approach for AE31 data had not been examined. We found a significant disagreement of $AAE_{880/950}$ between AE33 and AE31 data, as indicated by the poor R^2 values (0.01, Figure 6g&h) and diametrically different annual averages (1.75~1.98 for AE31 and 0.67~0.68 for AE33, Table 3). The discrepancy in $AAE_{880/950}$ between AE33

https://doi.org/10.5194/amt-2023-245
Preprint. Discussion started: 6 December 2023


Atmospheric Measurement Techniques Discussions

and AE31 may be associated with the difference in instrument design and filter material. It is widely recognized that the AAE of BC from fossil-fuel combustion is close to unity (Bond and Bergstrom, 2006). The $AAE_{880/950}$ from AE31 data is simply too high to represent AAE_{BC}. Another piece of evidence is the distinct monthly variations of AAE as shown in Figure 7 and Table S8. During the wet season (April to September), the prevailing wind of PRD is dominated by the oceanic air masses from the South, thus the AAE values are close to 1 (Figure 7) as the ambient samples were dominated by local emissions. During the dry season (October to March), north wind prevails and PRD was influenced by the long-range-transport air masses. As a result, elevated AAE values were observed during the dry season due to the influence of biomass burning and coal combustion from eastern and northern China. Among all the AAE values ($AAE_{470/660}$, $AAE_{370/880}$, $AAE_{880/950}$, $AAE_{370/950}$ and $AAE_{370-950}$), $AAE_{880/950}$ is the only one that lacks seasonality (Figure 7), confirming that $AAE_{880/950}$ can represent the AAE of BC from fossil-fuel combustion (AAE_{BC}) and not affected by biomass burning during the dry season. These results suggest that AAE_{BC} determination by $AAE_{880/950}$ is suitable for AE33 data but not suitable for AE31 data.

3.5 Comparison of secondary brown carbon light absorption estimation

Secondary brown carbon light absorption (b_{abs_BrCsec}) estimation by the MRS approach has been widely adopted in recent studies (Wang et al., 2019a; Liakakou et al., 2020; Zhu et al., 2021b; Wu et al., 2023). To date, the difference in b_{abs_BrCsec} determination between AE31 and AE33 has not been reported. With the year-long co-located AE33 and AE31 data, this study aims to investigate the inter-instrument agreement on b_{abs_BrCsec}. The annual average values of b_{abs_BrCsec} (1 hr data) obtained in this study were 2.16 ± 2.02 Mm^{-1} (AE31_V), 2.61 ± 2.35 Mm^{-1} (AE31_W) and 1.99 ± 1.97 Mm^{-1} (AE33) as shown in Table S9. For AE31 results, b_{abs_BrCsec} by Weingartner correction is higher than those by Virkkula correction. This result suggests that secondary brown carbon light absorption estimation is sensitive to the data correction algorithm. Since the b_{abs_BrCsec} of AE31_V agrees better with AE33 (Figure S6a, R^2=0.72) than AE31_W (Figure S6b, R^2=0.44), further comparisons are focused on AE31_V vs. AE33. As shown in Figure 8a, linear regression of AE33 vs. AE31 yields a slope of 0.78 and close-to-zero intercept (-0.04). The annual difference of arithmetic mean in b_{abs_BrCsec} is 13%. Most of the monthly difference of arithmetic mean in b_{abs_BrCsec} is within 20% (Figure 8b), except for May 2021 (39%). These results suggest that despite that the monthly difference of arithmetic mean in b_{abs_BrCsec} is typically ~20%, the b_{abs_BrCsec} between AE31 and AE33 is highly correlated and comparable.

https://doi.org/10.5194/amt-2023-245
Preprint. Discussion started: 6 December 2023

Atmospheric Measurement Techniques Discussions

As summarized in Table 4, both AE31 and AE33 were frequently used in literature, and the b_{abs_BrCsec} found in this study is similar to those found in Athens, Greece (2.77 ± 17.44 Mm^{-1}) (Liakakou et al., 2020), but lower than those found in Wuhan (4.9 Mm^{-1}) (Wang et al., 2021b) and Xi'an (34.9 Mm^{-1}) (Zhu et al., 2021b). China. Similar to the monthly variations of AAE, b_{abs_BrCsec} exhibits distinct seasonality, which is high in the dry season and low in the wet season. As shown in Figure 9, a positive dependency of $AAE_{370/880}$ on b_{abs_BrCsec} was observed, suggesting that the AAE of aerosols was strongly affected by the abundance of secondary brown carbon. The diurnal pattern of b_{abs_BrCsec} obtain in this study (Figure S7) is similar to previous studies (Wang et al., 2019a; Zhang et al., 2021a), which is low in daytime and high in nighttime. It is widely accepted that the daytime decrease of b_{abs_BrCsec} was largely associated with the photo-bleaching of brown carbon (Zhong and Jang, 2011; Li et al., 2023).

4. Conclusions and recommendations

A year-long colocated measurement comparison of a single-spot aethalometer (AE31) and a dual-spot aethalometer (AE33) was conducted in urban Guangzhou between 1 April 2021 and 31 March 2022. To minimize the interference of the filter loading effect, two data correction algorithms (Virkkula and Weingartner) were included in the comparison for AE31 data, while the instrument-embedded dual-spot correction was adopted for AE33 data. The main findings and recommendations of this study are summarized as follows:

- The eBC detection limits of AE33 were largely improved comparing to AE31(e.g. LOD_{eBC_AE33}=14.97 ng m^{-3} vs. LOD_{eBC_AE31}=52.2 ng m^{-3}, @ 1 hr, 880 nm). The improvement was more pronounced at high time resolution (e.g. LOD_{eBC_AE33}=96.57 ng m^{-3} vs. LOD_{eBC_AE31}=730.68 ng m^{-3}, @ 2 min, 880 nm).
- The eBC mass concentrations of the AE33 and AE31 were well correlated, with a R^2 of 0.97 and a slope of 1.20. The ~20% bias in the slope found in this study suggests that the AE33/AE31 slope could be site-specific. To maintain the consistency of the historical data of AE31, the eBC mass concentration of AE33 aethalometer was further adjusted by a second correction factor (C_{eBC}), which is the slope obtained in the comparison. The annual mean eBC obtained from 1 hr AE33 data were 2.35±1.37 and 1.96±1.14 μg m^{-3}, respectively, before and after eBC post-adjustment. The later value agrees well with the AE31 annual average (1.95±1.12 μg m^{-3}), and the AE33 vs. AE31 slope achieves 1.00 after eBC post-adjustment of AE33.

https://doi.org/10.5194/amt-2023-245
Preprint. Discussion started: 6 December 2023

Atmospheric Measurement Techniques Discussions

- By adopting the localized multi-scattering correction factor (AE31 C_{ref}=3.48, AE33 $C_{ref} = C_{AE33} \cdot C'$=1.39· 2.1=2.919) obtained from previous studies, the b_{abs} of AE33 agrees well with AE31, as evidenced by the close-to-unity regression slope and high R^2 of the 1 hr data. The b_{abs} agreement slightly varies by wavelengths (slope: 0.87~1.04, R^2:0.95~0.97) and by month, but such b_{abs} agreement variations are not sensitive to the correction schemes (Virkkula or Weingartner) for AE31.
- A variety of AAE values ($AAE_{470/660}$, $AAE_{370/880}$, $AAE_{880/950}$, $AAE_{370/950}$ and $AAE_{370-950}$) calculated using data from AE31_V, AE31_W and AE33 were compared. The AAE values are moderately correlated between AE33 and AE31 (R^2: 0.37~0.63), except for $AAE_{880/950}$. It is suggested that $AAE_{880/950}$ can be used for AAE_{BC} estimation (Zhang et al., 2019). $AAE_{880/950}$ by AE31 found in this study is too high and is not correlated with those of AE33 (R^2=0.01). These results suggest that AAE_{BC} determination by $AAE_{880/950}$ is suitable for AE33 data but not suitable for AE31 data.
- Secondary brown carbon light absorption (b_{abs_BrCsec}) estimation by the MRS approach is sensitive to the data correction algorithm for AE31 results, and b_{abs_BrCsec} by the Weingartner correction is higher than those by the Virkkula correction. It is found that b_{abs_BrCsec} of AE31_V agrees better with AE33 than AE31_W. The annual difference of arithmetic mean in b_{abs_BrCsec} between AE33 and AE31_V is 13%, with an R^2 of 0.72. Despite that monthly difference of arithmetic means in b_{abs_BrCsec} is typically ~20%, the b_{abs_BrCsec} between AE31 and AE33 is highly correlated and comparable, but such inter-instrument difference is not neglectable and should be taken into account for secondary brown carbon estimation.
- To ensure the data continuity in long-term aethalometer measurements when transiting from the older (AE31) to the newer (AE33) model in permanent global-climate and air-quality stations, site-specific C_{ref} and eBC correction factor are needed.

Data availability.

The data used in this study are available upon request from the corresponding author (wucheng.vip@foxmail.com).

Supplement.

The supplement related to this article is available online.

CRediT authorship contribution statement

Liangbin Wu: Formal analysis, Investigation, Data Curation, Visualization, Writing - Original Draft,

https://doi.org/10.5194/amt-2023-245
Preprint. Discussion started: 6 December 2023

Writing. **Cheng Wu:** Conceptualization, Methodology, Formal analysis, Investigation, Data Curation, Visualization, Writing - Original Draft, Writing - Review & Editing, Supervision, Project administration, Funding acquisition. **Tao Deng:** Resources. **Dui Wu:** Resources, Funding acquisition. **Mei Li:** Resources. **Yong Jie Li:** Writing - Review & Editing, Funding acquisition. **Zhen Zhou:** Resources, Funding acquisition.

Competing interests.

The contact author has declared that none of the authors has any competing interests.

Acknowledgments

This work was supported by the National Natural Science Foundation of China (Grant No. 42377089), Science and Technology Development Fund, Macau SAR (File No. 0023/2021/A1), Multi-Year Research grant (No. MYRG2022-00027-FST) from the University of Macau, and Special Fund Project for Science and Technology Innovation Strategy of Guangdong Province (Grant No.2019B121205004).

References:

Al-Abadleh, H. A.: Aging of atmospheric aerosols and the role of iron in catalyzing brown carbon formation, Environmental Science: Atmospheres, 1, 297-345, doi: https://doi.org/10.1039/D1EA00038A, 2021.

Andreae, M. O. and Gelencser, A.: Black carbon or brown carbon? The nature of light-absorbing carbonaceous aerosols, Atmos. Chem. Phys., 6, 3131-3148, doi: https://doi.org/10.5194/acp-6-3131-2006, 2006.

Arnott, W. P., Hamasha, K., Moosmuller, H., Sheridan, P. J., and Ogren, J. A.: Towards aerosol light-absorption measurements with a 7-wavelength Aethalometer: Evaluation with a photoacoustic instrument and 3-wavelength nephelometer, Aerosol. Sci. Technol., 39, 17-29, doi: https://doi.org/10.1080/027868290901972, 2005.

Asmi, E., Backman, J., Servomaa, H., Virkkula, A., Gini, M. I., Eleftheriadis, K., Müller, T., Ohata, S., Kondo, Y., and Hyvärinen, A.: Absorption instruments inter-comparison campaign at the Arctic Pallas station, Atmos. Meas. Tech., 14, 5397-5413, doi: https://doi.org/10.5194/amt-14-5397-2021, 2021.

Bernardoni, V., Ferrero, L., Bolzacchini, E., Forello, A. C., Gregorič, A., Massabò, D., Močnik, G., Prati, P., Rigler, M., Santagostini, L., Soldan, F., Valentini, S., Valli, G., and Vecchi, R.: Determination of Aethalometer multiple-scattering enhancement parameters and impact on source apportionment during the winter 2017/18 EMEP/ACTRIS/COLOSSAL campaign in Milan, Atmos. Meas. Tech., 14, 2919-2940, doi: https://doi.org/10.5194/amt-14-2919-2021, 2021.

Bond, T. C. and Bergstrom, R. W.: Light absorption by carbonaceous particles: An investigative review, Aerosol. Sci. Technol., 40, 27-67, doi: https://doi.org/10.1080/02786820500421521, 2006.

Bond, T. C., Doherty, S. J., Fahey, D. W., Forster, P. M., Berntsen, T., DeAngelo, B. J., Flanner, M. G., Ghan, S., Karcher, B., Koch, D., Kinne, S., Kondo, Y., Quinn, P. K.,

https://doi.org/10.5194/amt-2023-245
Preprint. Discussion started: 6 December 2023

Sarofim, M. C., Schultz, M. G., Schulz, M., Venkataraman, C., Zhang, H., Zhang, S., Bellouin, N., Guttikunda, S. K., Hopke, P. K., Jacobson, M. Z., Kaiser, J. W., Klimont, Z., Lohmann, U., Schwarz, J. P., Shindell, D., Storelvmo, T., Warren, S. G., and Zender, C. S.: Bounding the role of black carbon in the climate system: A scientific assessment, J. Geophys. Res., 118, 5380-5552, doi: https://doi.org/10.1002/jgrd.50171, 2013.

Coen, M. C., Weingartner, E., Apituley, A., Ceburnis, D., Fierz-Schmidhauser, R., Flentje, H., Henzing, J. S., Jennings, S. G., Moerman, M., Petzold, A., Schmid, O., and Baltensperger, U.: Minimizing light absorption measurement artifacts of the Aethalometer: evaluation of five correction algorithms, Atmos. Meas. Tech., 3, 457-474, doi: https://doi.org/10.5194/amt-3-457-2010, 2010.

Drinovec, L., Močnik, G., Zotter, P., Prévôt, A. S. H., Ruckstuhl, C., Coz, E., Rupakheti, M., Sciare, J., Müller, T., Wiedensohler, A., and Hansen, A. D. A.: The "dual-spot" Aethalometer: an improved measurement of aerosol black carbon with real-time loading compensation, Atmos. Meas. Tech., 8, 1965-1979, doi: https://doi.org/10.5194/amt-8-1965-2015, 2015.

Feng, Y., Ramanathan, V., and Kotamarthi, V. R.: Brown carbon: a significant atmospheric absorber of solar radiation?, Atmos. Chem. Phys., 13, 8607-8621, doi: https://doi.org/10.5194/acp-13-8607-2013, 2013.

Ferrero, L., Bernardoni, V., Santagostini, L., Cogliati, S., Soldan, F., Valentini, S., Massabò, D., Močnik, G., Gregorič, A., Rigler, M., Prati, P., Bigogno, A., Losi, N., Valli, G., Vecchi, R., and Bolzacchini, E.: Consistent determination of the heating rate of light-absorbing aerosol using wavelength- and time-dependent Aethalometer multiple-scattering correction, Sci. Total. Environ., 791, 148277, doi: https://doi.org/10.1016/j.scitotenv.2021.148277, 2021.

Gao, Y., Wang, Q., Li, L., Dai, W., Yu, J., Ding, L., Li, J., Xin, B., Ran, W., Han, Y., and Cao, J.: Optical properties of mountain primary and secondary brown carbon aerosols in summertime, Sci. Total. Environ., 806, 150570, doi: https://doi.org/10.1016/j.scitotenv.2021.150570, 2022.

Guo, Z., Yang, Y., Hu, X., Peng, X., Fu, Y., Sun, W., Zhang, G., Chen, D., Bi, X., Wang, X., and Peng, P.: The optical properties and in-situ observational evidence for the formation of brown carbon in clouds, Atmos. Chem. Phys., 22, 4827-4839, doi: https://doi.org/10.5194/acp-22-4827-2022, 2022.

Hansen, A. D. A., Rosen, H., and Novakov, T.: The Aethalometer - an Instrument for the Real-Time Measurement of Optical-Absorption by Aerosol-Particles, Sci. Total. Environ., 36, 191-196, doi: https://doi.org/10.1016/0048-9697(84)90265-1, 1984.

Helin, A., Virkkula, A., Backman, J., Pirjola, L., Sippula, O., Aakko-Saksa, P., Väätäinen, S., Mylläri, F., Järvinen, A., Bloss, M., Aurela, M., Jakobi, G., Karjalainen, P., Zimmermann, R., Jokiniemi, J., Saarikoski, S., Tissari, J., Rönkkö, T., Niemi, J. V., and Timonen, H.: Variation of Absorption Ångström Exponent in Aerosols From Different Emission Sources, J. Geophys. Res., 126, e2020JD034094, doi: https://doi.org/10.1029/2020JD034094, 2021.

Huang, R.-J., Yang, L., Cao, J., Chen, Y., Chen, Q., Li, Y., Duan, J., Zhu, C., Dai, W., Wang, K., Lin, C., Ni, H., Corbin, J. C., Wu, Y., Zhang, R., Tie, X., Hoffmann, T., O'Dowd, C., and Dusek, U.: Brown Carbon Aerosol in Urban Xi'an, Northwest China:

https://doi.org/10.5194/amt-2023-245
Preprint. Discussion started: 6 December 2023

The Composition and Light Absorption Properties, Environ. Sci. Technol., 52, 6825-6833, doi: https://doi.org/10.1021/acs.est.8b02386, 2018.

Ivančič, M., Gregorič, A., Lavrič, G., Alföldy, B., Ježek, I., Hasheminassab, S., Pakbin, P., Ahangar, F., Sowlat, M., Boddeker, S., and Rigler, M.: Two-year-long high-time-resolution apportionment of primary and secondary carbonaceous aerosols in the Los Angeles Basin using an advanced total carbon–black carbon (TC-BC(λ)) method, Sci. Total. Environ., 848, 157606, doi: https://doi.org/10.1016/j.scitotenv.2022.157606, 2022.

Jacobson, M. Z.: Isolating nitrated and aromatic aerosols and nitrated aromatic gases as sources of ultraviolet light absorption, J. Geophys. Res., 104, 3527-3542, doi: https://doi.org/10.1029/1998jd100054, 1999.

Jiang, X., Liu, D., Li, Q., Tian, P., Wu, Y., Li, S., Hu, K., Ding, S., Bi, K., Li, R., Huang, M., Ding, D., Chen, Q., Kong, S., Li, W., Pang, Y., and He, D.: Connecting the Light Absorption of Atmospheric Organic Aerosols with Oxidation State and Polarity, Environ. Sci. Technol., 56, 12873-12885, doi: https://doi.org/10.1021/acs.est.2c02202, 2022.

Jo, D. S., Park, R. J., Lee, S., Kim, S. W., and Zhang, X.: A global simulation of brown carbon: implications for photochemistry and direct radiative effect, Atmos. Chem. Phys., 16, 3413-3432, doi: https://doi.org/10.5194/acp-16-3413-2016, 2016.

Kim, S.-W., Ogren, J. A., Sheridan, P. J., Yoon, S.-C., Sharma, S., and Lin, N.-H.: Multiple scattering correction factor estimation for aethalometer aerosol absorption coefficient measurement, Aerosol. Sci. Technol., 53, 160-171, doi: https://doi.org/10.1080/02786826.2018.1555368, 2018.

Lack, D., Moosmüller, H., McMeeking, G., Chakrabarty, R., and Baumgardner, D.: Characterizing elemental, equivalent black, and refractory black carbon aerosol particles: a review of techniques, their limitations and uncertainties, Anal Bioanal Chem, 406, 99-122, doi: https://doi.org/10.1007/s00216-013-7402-3, 2014.

Lack, D. A. and Cappa, C. D.: Impact of brown and clear carbon on light absorption enhancement, single scatter albedo and absorption wavelength dependence of black carbon, Atmos. Chem. Phys., 10, 4207-4220, doi: https://doi.org/10.5194/acp-10-4207-2010, 2010.

Lack, D. A. and Langridge, J. M.: On the attribution of black and brown carbon light absorption using the Ångström exponent, Atmos. Chem. Phys., 13, 10535-10543, doi: https://doi.org/10.5194/acp-13-10535-2013, 2013.

Laing, J. R., Jaffe, D. A., and Sedlacek, I. I. I. A. J.: Comparison of Filter-based Absorption Measurements of Biomass Burning Aerosol and Background Aerosol at the Mt. Bachelor Observatory, Aerosol. Air. Qual. Res., 20, 663-678, doi: https://doi.org/10.4209/aaqr.2019.06.0298, 2020.

Laskin, A., Laskin, J., and Nizkorodov, S. A.: Chemistry of Atmospheric Brown Carbon, Chemical Reviews, 115, 4335-4382, doi: https://doi.org/10.1021/cr5006167, 2015.

Lee, A. K. Y., Zhao, R., Li, R., Liggio, J., Li, S.-M., and Abbatt, J. P. D.: Formation of Light Absorbing Organo-Nitrogen Species from Evaporation of Droplets Containing Glyoxal and Ammonium Sulfate, Environ. Sci. Technol., 47, 12819-12826, doi: https://doi.org/10.1021/es402687w, 2013.

https://doi.org/10.5194/amt-2023-245
Preprint. Discussion started: 6 December 2023

Lei, Y., Li, D., Lu, D., Zhang, T., Sun, J., Wang, X., Xu, H., and Shen, Z.: Insights into the roles of aerosol soluble iron in secondary aerosol formation, Atmos. Environ., 294, 119507, doi: https://doi.org/10.1016/j.atmosenv.2022.119507, 2023.

Li, C., Yan, F., Kang, S., Yan, C., Hu, Z., Chen, P., Gao, S., Zhang, C., He, C., Kaspari, S., and Stubbins, A.: Carbonaceous matter in the atmosphere and glaciers of the Himalayas and the Tibetan plateau: An investigative review, Environ. Int., 146, 106281, doi: https://doi.org/10.1016/j.envint.2020.106281, 2021.

Li, H., McMeeking, G. R., and May, A. A.: Development of a new correction algorithm applicable to any filter-based absorption photometer, Atmos. Meas. Tech., 13, 2865-2886, doi: https://doi.org/10.5194/amt-13-2865-2020, 2020.

Li, Q., Liu, D., Jiang, X., Tian, P., Wu, Y., Li, S., Hu, K., Liu, Q., Huang, M., Li, R., Bi, K., Kong, S., Ding, D., and Yu, C.: Concurrent photochemical whitening and darkening of ambient brown carbon, Atmos. Chem. Phys., 23, 9439-9453, doi: https://doi.org/10.5194/acp-23-9439-2023, 2023.

Liakakou, E., Kaskaoutis, D. G., Grivas, G., Stavroulas, I., Tsagkaraki, M., Paraskevopoulou, D., Bougiatioti, A., Dumka, U. C., Gerasopoulos, E., and Mihalopoulos, N.: Long-term brown carbon spectral characteristics in a Mediterranean city (Athens), Sci. Total. Environ., 708, 135019, doi: https://doi.org/10.1016/j.scitotenv.2019.135019, 2020.

Lian, X., Hu, X., Sun, W., Guo, Z., Tang, Y., Zhang, G., Bi, X., Wang, X., and Sheng, G.: Advances on the aqueous reaction between carbonyl compounds and reduced nitrogen-containing compounds and its contribution to brown carbon, Geochimica, 110-120, doi: https://doi.org/10.19700/j.0379-1726.2021.01.011, 2021.

Liang, Y., Wu, C., Jiang, S., Li, Y. J., Wu, D., Li, M., Cheng, P., Yang, W., Cheng, C., Li, L., Deng, T., Sun, J. Y., He, G., Liu, B., Yao, T., Wu, M., and Zhou, Z.: Field comparison of electrochemical gas sensor data correction algorithms for ambient air measurements, Sens. Actuators B Chem., 327, 128897, doi: https://doi.org/10.1016/j.snb.2020.128897, 2021.

Lin, P., Bluvshtein, N., Rudich, Y., Nizkorodov, S. A., Laskin, J., and Laskin, A.: Molecular Chemistry of Atmospheric Brown Carbon Inferred from a Nationwide Biomass Burning Event, Environ. Sci. Technol., 51, 11561–11570, doi: https://doi.org/10.1021/acs.est.7b02276, 2017.

Lin, Y.-C., Zhang, Y.-L., Xie, F., Fan, M.-Y., and Liu, X.: Substantial decreases of light absorption, concentrations and relative contributions of fossil fuel to light-absorbing carbonaceous aerosols attributed to the COVID-19 lockdown in east China, Environ. Pollut., 275, 116615, doi: https://doi.org/10.1016/j.envpol.2021.116615, 2021.

Replacement Filter Tape for the Magee Scientific Model AE33 Aethalometer®: http://www.mageesci.com/images/stories/docs/Magee_Scientific_Filter_Aethalometer_AE_Tape_Replacement_discussion.pdf, 2017.

Moise, T., Flores, J. M., and Rudich, Y.: Optical Properties of Secondary Organic Aerosols and Their Changes by Chemical Processes, Chemical Reviews, 115, 4400-4439, doi: https://doi.org/10.1021/cr5005259, 2015.

Moosmüller, H., Chakrabarty, R. K., and Arnott, W. P.: Aerosol light absorption and its measurement: A review, J Quant Spectrosc Radiat Transf, 110, 844-878, doi:

https://doi.org/10.1016/j.jqsrt.2009.02.035, 2009.

Qin, Y. M., Tan, H. B., Li, Y. J., Li, Z. J., Schurman, M. I., Liu, L., Wu, C., and Chan, C. K.: Chemical characteristics of brown carbon in atmospheric particles at a suburban site near Guangzhou, China, Atmos. Chem. Phys., 18, 16409-16418, doi: https://doi.org/10.5194/acp-18-16409-2018, 2018.

Qu, Y., Liu, H., Zhou, Y., Dai, W., Shi, J., Wang, N., Shi, Y., Zhu, C., Tsai, C., and Cao, J.: Spectral dependence of light absorption and direct radiative forcing of the TSP, PM10, PM2.5 and PM0.1 in a rural region of northwestern China, Atmos. Environ., 292, 119417, doi: https://doi.org/10.1016/j.atmosenv.2022.119417, 2023.

Rajesh, T. A. and Ramachandran, S.: Black carbon aerosol mass concentration, absorption and single scattering albedo from single and dual spot aethalometers: Radiative implications, J. Aerosol. Sci., 119, 77-90, doi: https://doi.org/10.1016/j.jaerosci.2018.02.001, 2018.

Rosen, H., Hansen, A. D. A., Dod, R. L., and Novakov, T.: Soot in Urban Atmospheres - Determination by an Optical-Absorption Technique, Science, 208, 741-744, doi: https://doi.org/10.1126/science.208.4445.741, 1980.

Savadkoohi, M., Pandolfi, M., Reche, C., Niemi, J. V., Mooibroek, D., Titos, G., Green, D. C., Tremper, A. H., Hueglin, C., Liakakou, E., Mihalopoulos, N., Stavroulas, I., Artiñano, B., Coz, E., Alados-Arboledas, L., Beddows, D., Riffault, V., De Brito, J. F., Bastian, S., Baudic, A., Colombi, C., Costabile, F., Chazeau, B., Marchand, N., Gómez-Amo, J. L., Estellés, V., Matos, V., van der Gaag, E., Gille, G., Luoma, K., Manninen, H. E., Norman, M., Silvergren, S., Petit, J.-E., Putaud, J.-P., Rattigan, O. V., Timonen, H., Tuch, T., Merkel, M., Weinhold, K., Vratolis, S., Vasilescu, J., Favez, O., Harrison, R. M., Laj, P., Wiedensohler, A., Hopke, P. K., Petäjä, T., Alastuey, A., and Querol, X.: The variability of mass concentrations and source apportionment analysis of equivalent black carbon across urban Europe, Environ. Int., 178, 108081, doi: https://doi.org/10.1016/j.envint.2023.108081, 2023.

Schmid, O., Artaxo, P., Arnott, W. P., Chand, D., Gatti, L. V., Frank, G. P., Hoffer, A., Schnaiter, M., and Andreae, M. O.: Spectral light absorption by ambient aerosols influenced by biomass burning in the Amazon Basin. I: Comparison and field calibration of absorption measurement techniques, Atmos. Chem. Phys., 6, 3443-3462, doi: https://doi.org/10.5194/acp-6-3443-2006, 2006.

Tang, M., Alexander, J. M., Kwon, D., Estillore, A. D., Laskina, O., Young, M. A., Kleiber, P. D., and Grassian, V. H.: Optical and Physicochemical Properties of Brown Carbon Aerosol: Light Scattering, FTIR Extinction Spectroscopy, and Hygroscopic Growth, The Journal of Physical Chemistry A, 120, 4155-4166, doi: https://doi.org/10.1021/acs.jpca.6b03425, 2016.

Titos, G., Lyamani, H., Drinovec, L., Olmo, F. J., Močnik, G., and Alados-Arboledas, L.: Evaluation of the impact of transportation changes on air quality, Atmos. Environ., 114, 19-31, doi: https://doi.org/10.1016/j.atmosenv.2015.05.027, 2015.

Virkkula, A., Makela, T., Hillamo, R., Yli-Tuomi, T., Hirsikko, A., Hameri, K., and Koponen, I. K.: A simple procedure for correcting loading effects of aethalometer data, J. Air. Waste. Manage., 57, 1214-1222, doi: https://doi.org/10.3155/1047-3289.57.10.1214, 2007.

https://doi.org/10.5194/amt-2023-245
Preprint. Discussion started: 6 December 2023

Wang, Q., Han, Y., Ye, J., Liu, S., Pongpiachan, S., Zhang, N., Han, Y., Tian, J., Wu, C., Long, X., Zhang, Q., Zhang, W., Zhao, Z., and Cao, J.: High Contribution of Secondary Brown Carbon to Aerosol Light Absorption in the Southeastern Margin of Tibetan Plateau, Geophys. Res. Lett., 46, 4962-4970, doi: https://doi.org/10.1029/2019gl082731, 2019a.

Wang, Q., Ye, J., Wang, Y., Zhang, T., Ran, W., Wu, Y., Tian, J., Li, L., Zhou, Y., Hang Ho, S. S., Dang, B., Zhang, Q., Zhang, R., Chen, Y., Zhu, C., and Cao, J.: Wintertime Optical Properties of Primary and Secondary Brown Carbon at a Regional Site in the North China Plain, Environ. Sci. Technol., 53, 12389-12397, doi: https://doi.org/10.1021/acs.est.9b03406, 2019b.

Wang, Q., Liu, H., Ye, J., Tian, J., Zhang, T., Zhang, Y., Liu, S., and Cao, J.: Estimating Absorption Ångström Exponent of Black Carbon Aerosol by Coupling Multiwavelength Absorption with Chemical Composition, Environmental Science & Technology Letters, 8, 121-127, doi: https://doi.org/10.1021/acs.estlett.0c00829, 2021a.

Wang, Q., Wang, L., Tao, M., Chen, N., Lei, Y., Sun, Y., Xin, J., Li, T., Zhou, J., Liu, J., Ji, D., and Wang, Y.: Exploring the variation of black and brown carbon during COVID-19 lockdown in megacity Wuhan and its surrounding cities, China, Sci. Total. Environ., 791, 148226, doi: https://doi.org/10.1016/j.scitotenv.2021.148226, 2021b.

Wang, X., Heald, C. L., Ridley, D. A., Schwarz, J. P., Spackman, J. R., Perring, A. E., Coe, H., Liu, D., and Clarke, A. D.: Exploiting simultaneous observational constraints on mass and absorption to estimate the global direct radiative forcing of black carbon and brown carbon, Atmos. Chem. Phys., 14, 10989-11010, doi: https://doi.org/10.5194/acp-14-10989-2014, 2014.

Weingartner, E., Saathoff, H., Schnaiter, M., Streit, N., Bitnar, B., and Baltensperger, U.: Absorption of light by soot particles: determination of the absorption coefficient by means of aethalometers, J. Aerosol. Sci., 34, 1445-1463, doi: https://doi.org/10.1016/S0021-8502(03)00359-8, 2003.

WMO/GAW: WMO/GAW Aerosol Measurement Procedures, Guidelines and Recommendations, 2016.

Wu, C. and Yu, J. Z.: Determination of primary combustion source organic carbon-to-elemental carbon (OC/EC) ratio using ambient OC and EC measurements: secondary OC-EC correlation minimization method, Atmos. Chem. Phys., 16, 5453-5465, doi: https://doi.org/10.5194/acp-16-5453-2016, 2016.

Wu, C., Wu, D., and Yu, J. Z.: Quantifying black carbon light absorption enhancement with a novel statistical approach, Atmos. Chem. Phys., 18, 289-309, doi: https://doi.org/10.5194/acp-18-289-2018, 2018.

Wu, C. and Yu, J. Z.: Evaluation of linear regression techniques for atmospheric applications: the importance of appropriate weighting, Atmos. Meas. Tech., 11, 1233-1250, doi: https://doi.org/10.5194/amt-11-1233-2018, 2018.

Wu, C., He, C., Brown, Z. E., Miljevic, B., Zhang, C., Wang, H., Wang, B., Morawska, L., and Ristovski, Z.: Light absorption properties of black and brown carbon during the prescribed burning season at an urban background site in Brisbane, Australia, Atmos. Environ., 313, 120072, doi: https://doi.org/10.1016/j.atmosenv.2023.120072, 2023.

Wu, D., Wu, C., Liao, B., Chen, H., Wu, M., Li, F., Tan, H., Deng, T., Li, H., Jiang, D.,

https://doi.org/10.5194/amt-2023-245
Preprint. Discussion started: 6 December 2023

690 and Yu, J. Z.: Black carbon over the South China Sea and in various continental locations in South China, Atmos. Chem. Phys., 13, 12257-12270, doi: https://doi.org/10.5194/acp-13-12257-2013, 2013.

Yus-Díez, J., Bernardoni, V., Močnik, G., Alastuey, A., Ciniglia, D., Ivančič, M., Querol, X., Perez, N., Reche, C., Rigler, M., Vecchi, R., Valentini, S., and Pandolfi, M.: 695 Determination of the multiple-scattering correction factor and its cross-sensitivity to scattering and wavelength dependence for different AE33 Aethalometer filter tapes: a multi-instrumental approach, Atmos. Meas. Tech., 14, 6335-6355, doi: https://doi.org/10.5194/amt-14-6335-2021, 2021.

Zhang, G. H., Peng, L., Lian, X. F., Lin, Q. H., Bi, X. H., Chen, D. H., Li, M., Li, L., 700 Wang, X. M., and Sheng, G. Y.: An Improved Absorption Angstrom Exponent (AAE)-Based Method for Evaluating the Contribution of Light Absorption from Brown Carbon with a High-Time Resolution, Aerosol. Air. Qual. Res., 19, 15-24, doi: https://doi.org/10.4209/aaqr.2017.12.0566, 2019.

Zhang, Q., Shen, Z., Zhang, L., Zeng, Y., Ning, Z., Zhang, T., Lei, Y., Wang, Q., Li, G., 705 Sun, J., Westerdahl, D., Xu, H., and Cao, J.: Investigation of Primary and Secondary Particulate Brown Carbon in Two Chinese Cities of Xi'an and Hong Kong in Wintertime, Environ. Sci. Technol., 54, 3803–3813, doi: https://doi.org/10.1021/acs.est.9b05332, 2020.

Zhang, Q., Shen, Z., Zhang, T., Kong, S., Lei, Y., Wang, Q., Tao, J., Zhang, R., Wei, P., 710 Wei, C., Cui, S., Cheng, T., Ho, S. S. H., Li, Z., Xu, H., and Cao, J.: Spatial distribution and sources of winter black carbon and brown carbon in six Chinese megacities, Sci. Total. Environ., 762, 143075, doi: https://doi.org/10.1016/j.scitotenv.2020.143075, 2021a.

Zhang, Y., Zhi, G., Jin, W., Liu, S., Wang, L., Li, Z., Shi, R., Zhang, P., Shu, Y., and Hu, 715 J.: Developing a dynamic correction mechanism for aethalometer results of actual urban aerosols, Atmos. Res., 255, 105529, doi: https://doi.org/10.1016/j.atmosres.2021.105529, 2021b.

Zhao, G., Yu, Y., Tian, P., Li, J., Guo, S., and Zhao, C.: Evaluation and Correction of the Ambient Particle Sectral Light Absorption Measured Using a Filter-based 720 Aethalometer, Aerosol. Air. Qual. Res., 20, 1833–1841, doi: https://doi.org/10.4209/aaqr.2019.10.0500, 2020.

Zheng, H., Kong, S., Chen, N., Fan, Z., Zhang, Y., Yao, L., Cheng, Y., Zheng, S., Yan, Y., Liu, D., Zhao, D., Liu, C., Zhao, T., Guo, J., and Qi, S.: A method to dynamically constrain black carbon aerosol sources with online monitored potassium, NPJ Clim. 725 Atmos. Sci., 4, 43, doi: https://doi.org/10.1038/s41612-021-00200-y, 2021.

Zhong, M. and Jang, M.: Light absorption coefficient measurement of SOA using a UV–Visible spectrometer connected with an integrating sphere, Atmos. Environ., 45, 4263-4271, doi: https://doi.org/10.1016/j.atmosenv.2011.04.082, 2011.

Zhu, C.-S., Qu, Y., Huang, H., Chen, J., Dai, W.-T., Huang, R.-J., and Cao, J.-J.: Black 730 Carbon and Secondary Brown Carbon, the Dominant Light Absorption and Direct Radiative Forcing Contributors of the Atmospheric Aerosols Over the Tibetan Plateau, Geophys. Res. Lett., 48, e2021GL092524, doi: https://doi.org/10.1029/2021GL092524, 2021a.

https://doi.org/10.5194/amt-2023-245
Preprint. Discussion started: 6 December 2023

Zhu, C.-S., Qu, Y., Zhou, Y., Huang, H., Liu, H.-K., Yang, L., Wang, Q.-Y., Hansen, A. D. A., and Cao, J.-J.: High light absorption and radiative forcing contributions of primary brown carbon and black carbon to urban aerosol, Gondwana Research, 90, 159-164, doi: https://doi.org/10.1016/j.gr.2020.10.016, 2021b.

https://doi.org/10.5194/amt-2023-245
Preprint. Discussion started: 6 December 2023

Atmospheric Measurement Techniques Discussions

Table 1. Summary of existing AE31/AE33 intercomparison studies.

Measurement site	Model	Time base	Flow rate (LPM)	Filter	Period (duration)	Slope (AE33 vs AE31)	Reference
Ahmedabad, India (urban)	AE31	5 min	3	Quartz fiber filter C_{ref}= 2.14	July 2014 – Dec 2014	eBC_{880}	(Rajesh and Ramachandran, 2018)
	AE33	1 min	3	Teflon coated glass fiber C_{AE33}= 1.57	6 months	5 min :1.06 1 hr: 1.02	
Milan, Italy (urban)	AE31	5 min		Quartz fiber filter (Pallflex Q250F)	Jan. 18 – Feb. 15 (2018)	eBC_{880}	(Ferrero et al., 2021)
	AE33	1 min		Teflon-coated glass fiber (Pallflex T60A20) C_{AE33}= 1.57	1 month	5 min: 1.05	
Granada, Spain (urban)	AE31	5 min			June 2014 – July 2014	eBC_{880} 5 min: 1.11	(Titos et al., 2015)
	AE33	1 min			2 months		
Pallas, Finland (background)	AE31	5 min	4.5	C_{ref}= 3.5	June. 19 – July. 17 (2019)	b_{abs660} 1 hr: 0.47	(Asmi et al., 2021)
	AE33	1 min	5.8	C_{AE33}=1.39 C'=2.52	1 month		
Guangzhou, China (urban)	AE31	5 min	2.4	Quartz-fiber filter (Pallflex Q250F) C_{ref}= 3.48	Apr 2021 – Mar 2022	eBC_{880} 5 min: 1.18 1 hr: 1.20	This study
	AE33	1 min	3	M8060 C_{AE33}=1.39 C'=2.1	12 months	b_{abs880} 5 min: 0.85-0.86 1 hr: 0.87	

740

https://doi.org/10.5194/amt-2023-245
Preprint. Discussion started: 6 December 2023

Atmospheric Measurement Techniques Discussions

Table 2. The eBC LOD (ng m^{-3}) of AE31 and AE33 at different time bases at seven wavelengths. N refers to the number of data points.

Model	Time base	370 nm	470 nm	520 nm	590 nm	660 nm	880 nm	950 nm	N
AE33	1 s	533.67	601.89	662.34	706.68	807.51	1177.56	1234.95	345600
	1 min	82.17	62.37	68.28	79.98	86.07	112.71	118.17	5760
	2 min	75.42	52.53	57.78	67.23	74.04	96.57	99.72	2880
	4 min	66.06	44.43	48.51	56.88	62.55	81.75	83.55	1440
	10 min	37.38	24.87	27.30	31.86	34.77	45.66	46.05	576
	60 min	14.25	9.00	9.78	11.13	11.58	14.97	14.88	96
AE31	2 min	197.01	299.64	368.67	459.24	533.34	730.68	789.99	2880
	4 min	164.25	244.29	299.19	375.51	431.34	594.42	645.72	1440
	10 min	77.07	115.83	135.69	165.24	195.99	263.4	290.58	576
	30 min	31.17	45.39	48.42	55.62	64.08	79.53	105.93	192
	60 min	20.82	28.29	30.78	36.39	43.29	52.20	71.10	96

745

https://doi.org/10.5194/amt-2023-245
Preprint. Discussion started: 6 December 2023

Atmospheric Measurement Techniques Discussions

Table 3. The absorption Ångström exponent (AAE) of AE31 and AE33 aethalometers at 5 min and 1 hr time bases. Where "/" denotes the AAE value calculated by the light absorption coefficients of two wavelengths and "-" denotes the AAE value obtained from the curve fitting of the power function using all wavelengths within the said range.

AAE	Time base	AE31_V	AE31_W	AE33
$AAE_{470/660}$	1 hr	1.12 ± 0.15	1.08 ± 0.17	1.33 ± 0.12
	5 min	1.12 ± 0.34	1.09 ± 0.35	1.34 ± 0.14
$AAE_{370/880}$	1 hr	1.11 ± 0.14	1.05 ± 0.17	1.20 ± 0.13
	5 min	1.12 ± 0.24	1.05 ± 0.26	1.20 ± 0.14
$AAE_{880/950}$	1 hr	1.75 ± 0.47	1.94 ± 0.46	0.67 ± 0.12
	5 min	1.81 ± 1.02	1.98 ± 1.03	0.68 ± 0.22
$AAE_{370/950}$	1 hr	1.16 ± 0.14	1.12 ± 0.17	1.15 ± 0.12
	5 min	1.17 ± 0.28	1.12 ± 0.29	1.15 ± 0.13
$AAE_{370-950}$	1 hr	1.11 ± 0.12	1.07 ± 0.15	1.19 ± 0.12
	5 min	1.14 ± 0.27	1.10 ± 0.28	1.19 ± 0.13

750

https://doi.org/10.5194/amt-2023-245
Preprint. Discussion started: 6 December 2023

Atmospheric Measurement Techniques Discussions

Table 4. Summary of secondary brown carbon light absorption reported in the literature.

Location	Model	Sampling period	secondary brown carbon light absorption (b_{abs_BrCsec}) Mm^{-1}					Reference
			370 nm	470 nm	520 nm	590 nm	660 nm	
Guangzhou, China urban site	AE33	2021.04–2022.03	1.99 ± 1.97	0.91 ± 0.84	0.67 ± 0.59	0.45 ± 0.41	0.27 ± 0.24	This study
		Dry season	2.34 ± 2.08	1.12 ± 0.86	1.05 ± 0.69	0.56 ± 0.43	0.34 ± 0.26	
		Wet season	0.99 ± 1.15	0.38 ± 0.45	0.40 ± 0.29	0.23 ± 0.23	0.13 ± 0.12	
	AE31_V	2021.04–2022.03	2.16 ± 2.02	1.10 ± 0.97	0.72 ± 0.60	0.45 ± 0.37	0.37 ± 0.34	
		Dry season	2.68 ± 2.15	1.38 ± 1.03	0.93 ± 0.64	0.57 ± 0.39	0.46 ± 0.37	
		Wet season	1.12 ± 1.15	0.55 ± 0.52	0.39 ± 0.34	0.24 ± 0.21	0.22 ± 0.20	
Athens, Greece urban site	AE33	2015.5–2019.4	2.77 ± 17.44	0.69 ± 4.94	0.61 ± 3.63	0.16 ± 1.25	0.47 ± 1.73	(Liakakou et al., 2020)
Xianghe, China rural site	AE33	2017.12–2018.1	11.8	8.8	6.2	4.3	3.3	(Wang et al., 2019b)
Wuhan, China urban site	AE31	2020.1	4.9 ± 4.6	/	/	/	/	(Wang et al., 2021b)
Xi'an, China urban site	AE33	2015.11–2016.2	34.9	11.4	5.6	3.5	2.3	(Zhu et al., 2021b)
Xi'an, China urban site	AE31	2016.12.16–2017.1.15	25.8	4.0	3.7	2.4	1.4	(Zhang et al., 2020)
Hong Kong, China urban site		2016.12.16–2017.1.15	4.8	3.4	2.4	1.7	1.2	
Qinghai Lake, China, rural site	AE33	2019.11–2020.2	7.9	2.2	1.0	0.6	0.3	(Zhu et al., 2021a)
Shaanxi, China Mount Hua	AE33	2018.8	4.4 ± 6.1	/	/	/	/	(Gao et al., 2022)
Guanzhong Plain, China, rural site	AE31	2015.12–2016.1	3.1	1.5	0.3	0.1	0.4	(Qu et al., 2023)
Brisbane, Australia urban site	AE31	2022.7–9	1.4	0.6	0.5	0.2	0.3	(Wu et al., 2023)
Tibetan Plateau, China, rural site	AE33	2018.3–5	6.9	5.7	4.1	3.6	2.1	(Wang et al., 2019a)
Nanjing, China urban site	AE33	2020.1–3	3.7 ± 4	2.0 ± 2	1.7 ± 1	1.0 ± 0.8	0.4 ± 0.5	(Lin et al., 2021)

https://doi.org/10.5194/amt-2023-245
Preprint. Discussion started: 6 December 2023

Atmospheric Measurement Techniques Discussions

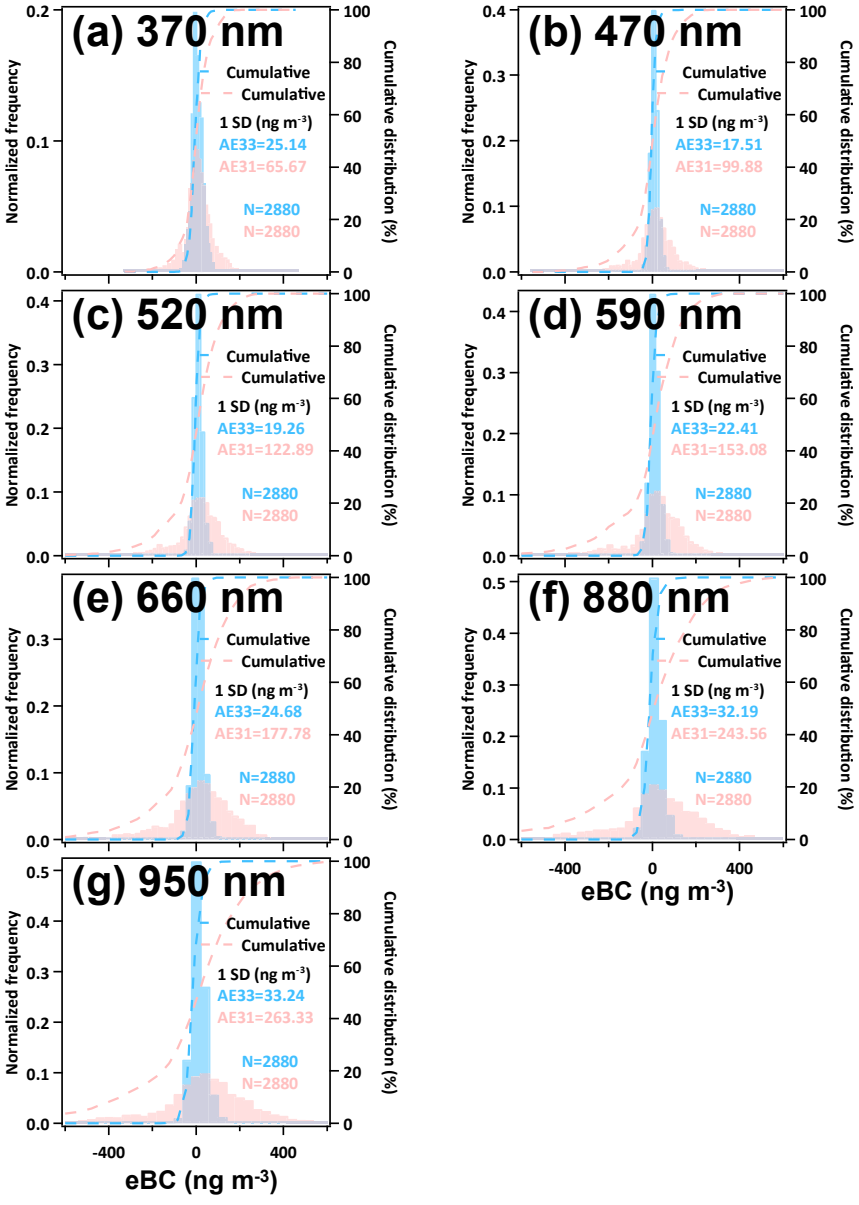

755 **Figure 1.** The frequency distributions of blank measurements of AE31 and AE33 at the time base of 2 min. The red histograms represent AE31and AE33 results are shown in blue histograms. Figures a-g correspond to 370, 470, 520, 590, 660, 880 and 950 nm, respectively.

https://doi.org/10.5194/amt-2023-245
Preprint. Discussion started: 6 December 2023

Atmospheric Measurement Techniques Discussions

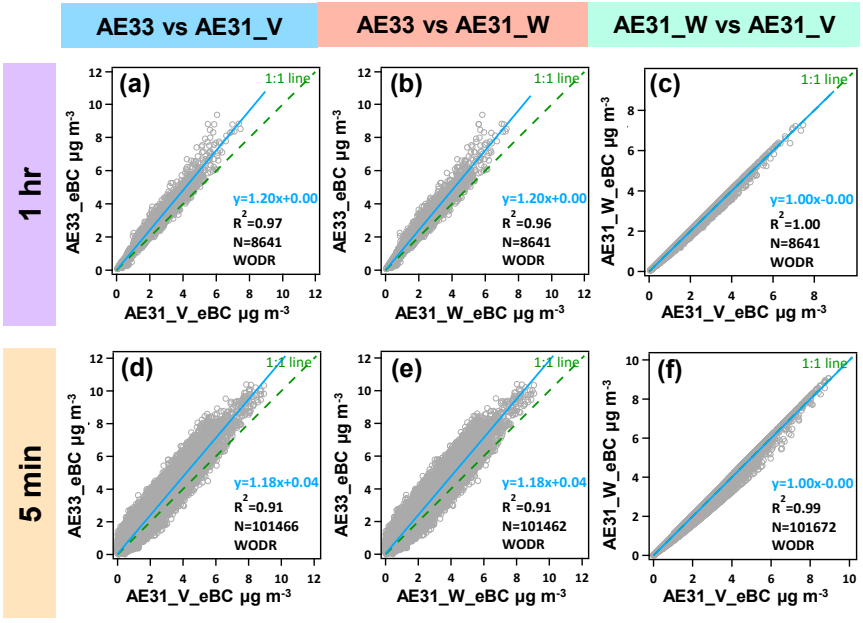

760 **Figure 2.** Comparisons of 5 min and 1 hr eBC mass concentrations at 880 nm between AE33 and AE31. AE31_V_eBC and AE31_W_eBC are the eBC mass concentrations of AE31 corrected by Virkkula and Weingartner algorithms, respectively. AE33_eBC represents the eBC mass concentration of AE33 at 880 nm.

https://doi.org/10.5194/amt-2023-245
Preprint. Discussion started: 6 December 2023

Atmospheric Measurement Techniques Discussions

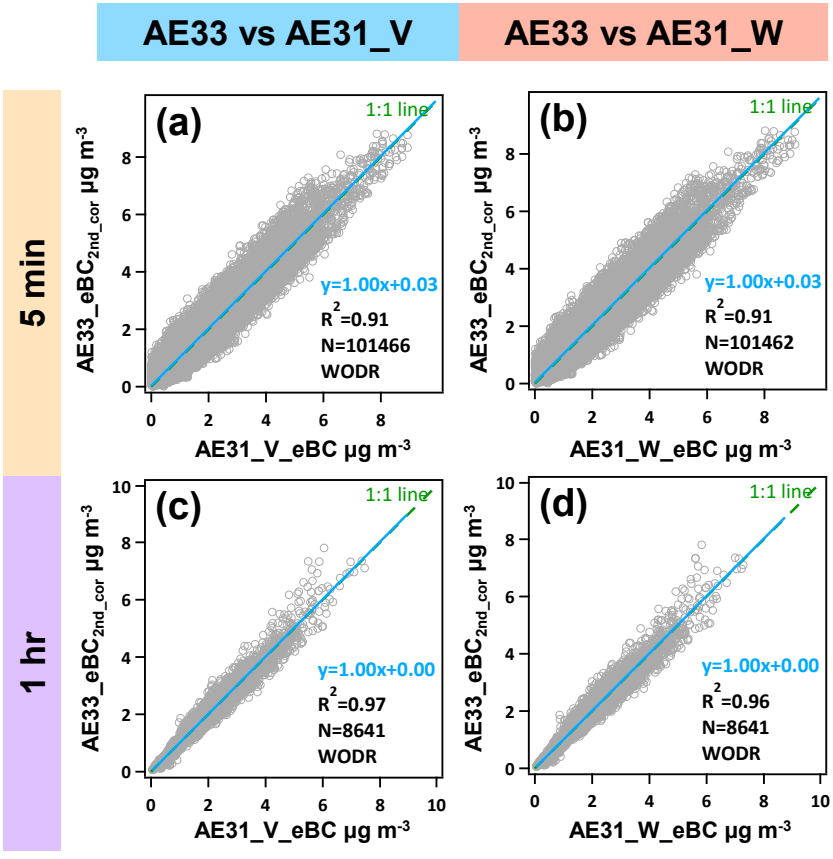

765

Figure 3. The 2nd-correction eBC mass concentration comparison between AE33 data and AE31 data at 5 min and 1 hr time base.

https://doi.org/10.5194/amt-2023-245
Preprint. Discussion started: 6 December 2023

Atmospheric Measurement Techniques Discussions

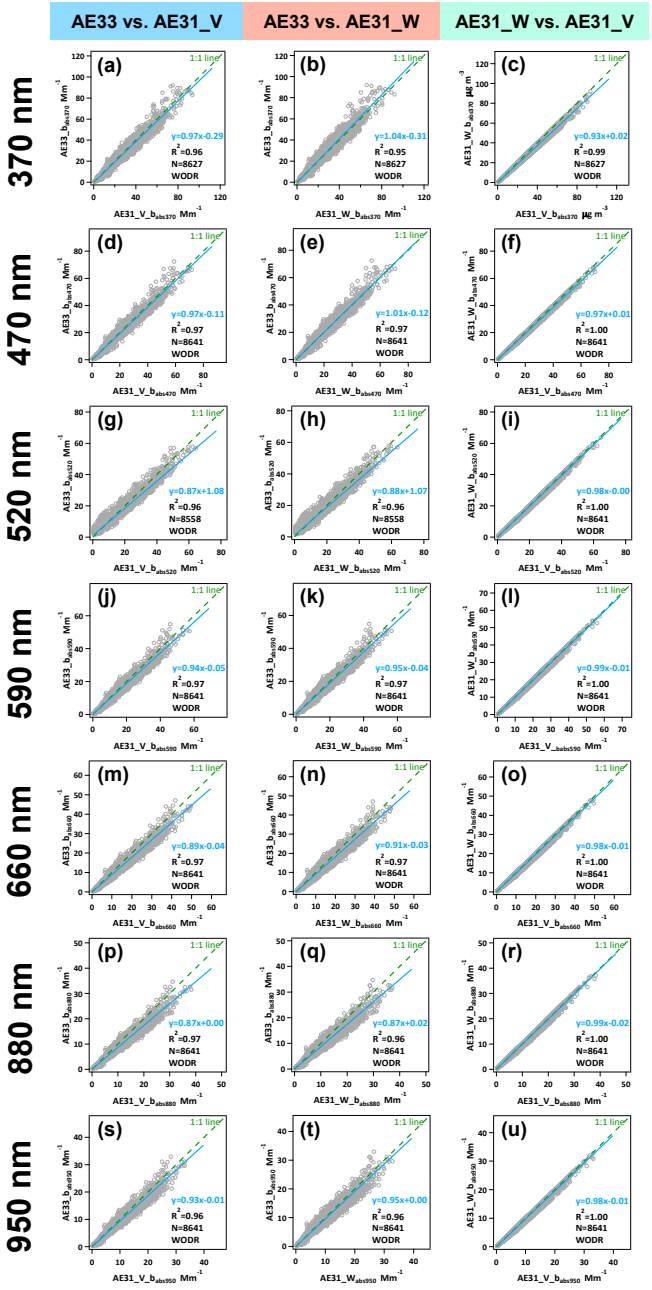

770 **Figure 4**. Comparison of hourly light absorption coefficient between AE33 and AE31 at 370, 470, 520, 590, 660, 880 and 950 nm. AE31_V_b_{abs} and AE31_W_b_{abs} represent light absorption coefficients of AE31 corrected by Virkkula and Weingartner algorithms, respectively.

https://doi.org/10.5194/amt-2023-245
Preprint. Discussion started: 6 December 2023

Atmospheric Measurement Techniques Discussions

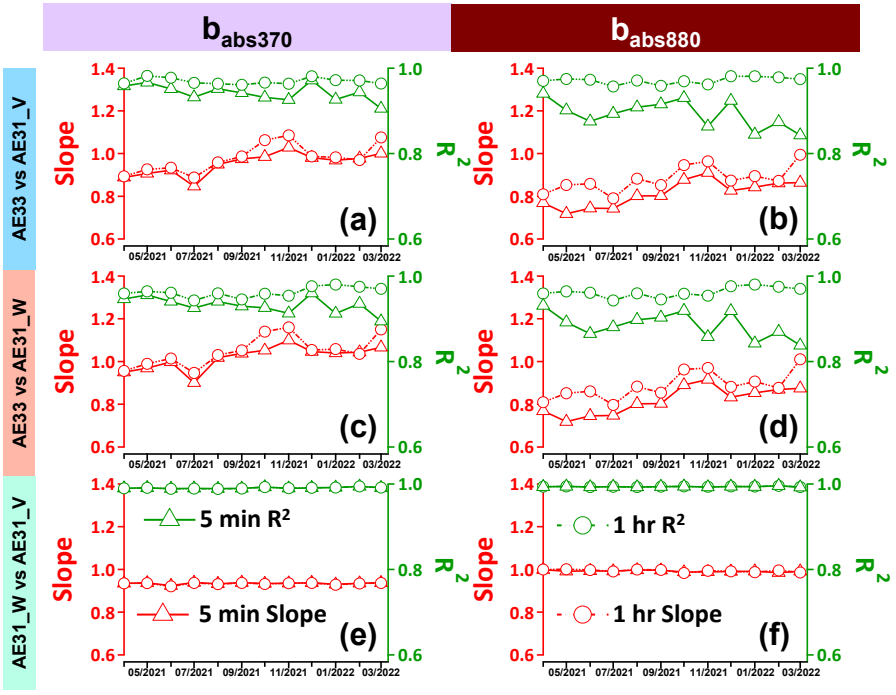

Figure 5. Monthly variation of slope and R^2 of AE33 and AE31 comparisons at 5 min and 1 hr time resolutions.

https://doi.org/10.5194/amt-2023-245
Preprint. Discussion started: 6 December 2023

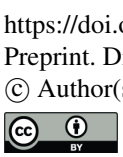

Atmospheric Measurement Techniques Discussions

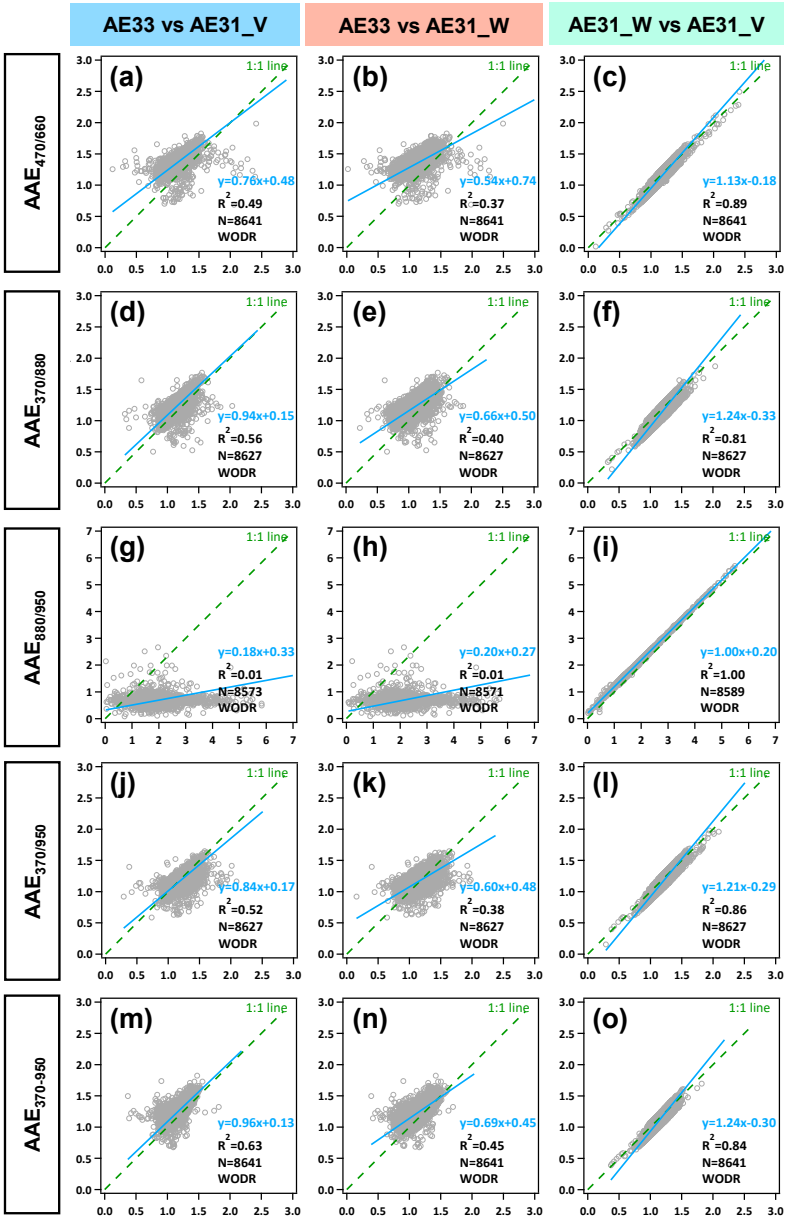

Figure 6. Inter-instrument comparison of different AAE values ($AAE_{470/660}$, $AAE_{370/880}$, $AAE_{880/950}$, $AAE_{370/950}$ and $AAE_{370-950}$) calculated using 1-hr data from AE31_V, AE31_W and AE33.

780

https://doi.org/10.5194/amt-2023-245
Preprint. Discussion started: 6 December 2023

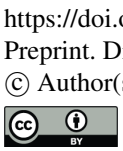

Atmospheric Measurement Techniques Discussions

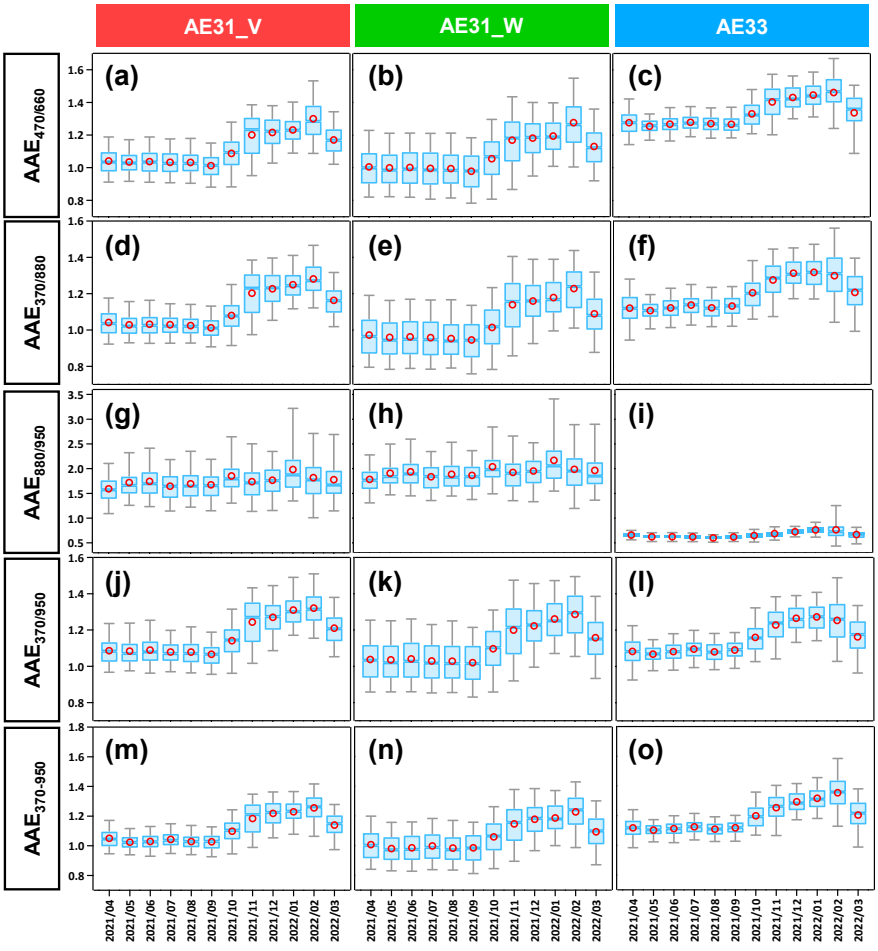

Figure 7. Monthly variations of different AAE values ($AAE_{470/660}$, $AAE_{370/880}$, $AAE_{880/950}$, $AAE_{370/950}$ and $AAE_{370-950}$) calculated using 1-hr data from AE31_V, AE31_W and AE33.

https://doi.org/10.5194/amt-2023-245
Preprint. Discussion started: 6 December 2023

Atmospheric Measurement Techniques Discussions

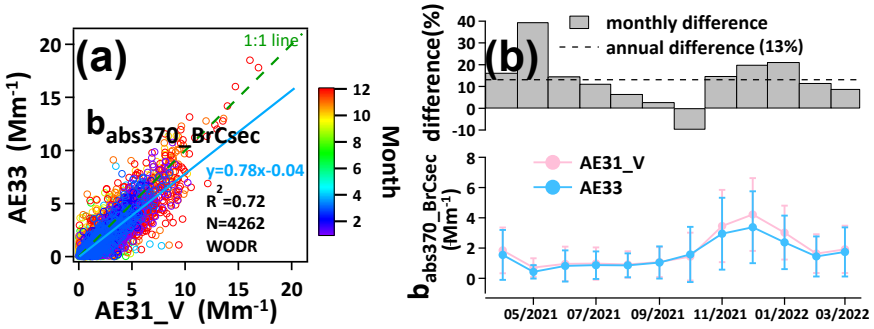

785

Figure 8. Comparison of secondary brown carbon light absorption at 370 nm (b_{abs370_BrCsec}) estimated by AE33 and AE31_V (AE31 data correction using Virkkula algorithm). (a) Scatter plot of hourly b_{abs370_BrCsec} comparison between AE33 and AE31_V. The color coding represents months. (b) Monthly comparison of b_{abs370_BrCsec} between AE33 and AE31_V.

790

https://doi.org/10.5194/amt-2023-245
Preprint. Discussion started: 6 December 2023

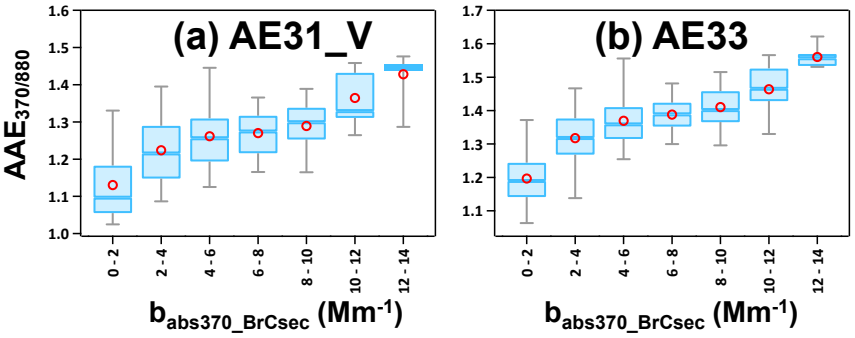

Figure 9. Dependence of $AAE_{370/880}$ on b_{abs370_BrCsec}. $AAE_{370/880}$ is the absorption Ångström exponent calculated from the light absorption at 370 and 880 nm, while b_{abs370_BrCsec} is the secondary brown carbon light absorption at 370 nm. These figures were visualized using the Igor-based toolkit Histbox (Wu et al., 2018).